Controlling Non-reciprocity using Enhanced Brillouin Scattering

Sameh Y. Elnaggar, *Member, IEEE,* and Gregory N. Milford, *Member, IEEE*

***Abstract*—The properties of space-time modulated media operating in the sub-sonic regime are discussed based on rigorous Bloch-Floquet theory. A geometrical description in the frequency-wavenumber plane is developed to provide insight into the possible interactions and their nature. It is shown that the secular equation has a singularity, which results in a weak/passive second harmonic generation process. Additionally bandgaps arising from the strong/active parametric interaction between an incident wave and its space-time harmonic, result in an inelastic Brillouin like scattering process. Hence when the incident frequency is inside a forward (backward) bandgap, a Stokes' (Anti-Stokes') scattered wave bounces back to the source. Although the forward and backward bandgaps do not generally occur at the same frequency bands, the insertion loss and gap width are equal. Requiring that both gaps do not overlap, enforces a lower bound on the modulation speed. It is shown that although an increase in the modulation index is desirable, as it enhances the non-reciprocal behaviour, it also limits the range of possible modulation speeds. It is shown that an alternative way to enhance the nonreciprocity, whenever the modulation index is constrained, is through the reduction of the modulation wavelength. The effective complex refractive index is calculated over a wide frequency range. It is shown that peaks appear in the extinction coefficient, indicating scattering to Stokes' and Anti-Stokes' waves. Finally, a comprehensive numerical analysis based on the Finite Difference Time Domain method is developed to verify and demonstrate the intriguing properties of space-time modulated media.**

***Index Terms*—Periodic structures, Distributed parameter circuits, Active circuits, Microwave photonics, Time-varying systems, Multiwave mixing, Optical harmonic generation, Dispersion, Metamaterials, Electromagnetic propagation, Finite difference methods.**

I. Introduction

The study of space-time modulated media sparked interest in the late 1950s and early 1960s in the exploration of the properties of travelling wave parametric amplifiers [1]–[6]. In these systems, a strong wave (the pump) modulates a system parameter; for instance a varactor-loaded transmission line can be space-time modulated via the introduction of a strong pump wave that modulates the capacitance value in both space and time. A general solution of the system is determined by a wave and all its infinite space-time harmonics as dictated by the Bloch-Floquet Theorem. Traditionally whenever the modulation index is significantly small, the propagation behaviour can be explained using the *parametric* interaction of two waves: the signal and idler. This is equivalent to truncating the space-time harmonics expansion to two terms only. This approach, also known as three wave mixing, is widely used to describe nonlinear behaviours in optical media, such as parametric generation and inelastic scattering [7], [8]. In an early work, Slater pointed out to the common features between space-time modulated media and scattering from crystals [9]. Recently we showed that the dynamical behaviour of a sinusoidally pumped nonlinear composite right left handed transmission line (NL CRLH TL) resembles a Stimulated Brilliouin Scattering process observed in crystal structures [7], [10].

Despite the success of three wave mixing in describing scattering in nonlinear optical media, its general application to any modulated media may lead to inaccurate results. For example Oliner et al showed that, whenever the speed of modulation is close enough to the speed of the unmodulated medium (in a dispersion-less medium), the full Bloch-Floquet modes must be used [4]. They based their arguments on a rigorous mathematical framework that they developed earlier to describe wave propagation in the presence of a spatially modulated surface reactance [11]. Very recently we showed that for a NL CRLH TL, three wave mixing does not provide accurate results for strong nonlinearity and/or the TL is relatively short [12].

Quite recently there has been renewed interest in space-time modulated structures for their non-reciprocal behaviour. It has previously been shown that the dispersion relation of a medium loses its symmetry once it is space-time modulated. In this case, waves travelling in the forward and backward directions do not necessary have the same wave number (i.e $\beta^F(\omega) \neq -\beta^B(\omega)$, F and B stand for forward and backward propagation, respectively) [5]. However, such intriguing behaviour has not been exploited until recently. For instance to obtain an optical isolation in one direction, non-reciprocity was introduced via the space-time modulation of the refractive index of a photonic crystal [13]. This imparts frequency and wave number shifts during a photonic indirect interband transition. The transition is made possible in a given direction by allowing the space-time modulation to phase match the frequencies and wave number of the incident wave and a crystal mode. This is equivalent to saying that both photons energy and momentum are simultaneously conserved. By properly choosing the length of the crystal to be equal to the coherence length, efficient transfer from the incident wave to its space-time harmonic can be made possible. In the opposite direction of propagation, however, the phase matching conditions are not satisfied; hence a photonic transition does not occur and propagation is not disturbed. The non-reciprocity via interband transition can be induced using an electrically driven photonic crystal [14].

S. Elnaggar and G. Milford are with the School of Engineering and Information Technology, University of New South Wales, Canberra, ACT, 2600 Australia e-mails: samehelnaggar@gmail.com and g.milford@adfa.edu.au

Using the metamaterial paradigm, space-time modulation was also exploited to introduce non-reciprocity on the meta-atomic level scale by mimicking Faraday's rotation. This was achieved by lifting mode azimuthal degeneracy in a ring resonator via the space time modulation of the dielectric constant [15]. The modulation frequency ω_m allows the clock and anti-clock modes to resonant couple. The coupling process, analyzed by coupled mode theory [16], is mediated by the modulated dielectric constant. As a result, the coupled (hybridized) modes are different in character and as a consequence non-reciprocity arises.

In essence, the introduction of space-time modulation biases the system, leading to an asymmetric coupling of the space-time harmonics, which results in the non-reciprocal behaviour. This property was recently utilized to break time-reversal symmetry. Such property was exploited to design a multitude of interesting devices; for example: non-reciprocal leaky wave antenna [17], [18], circulators [19], [20], isolators [21] and potential novel devices such as metasurfaces [22].

In the context of an elastic media, it was shown that by properly choosing the modulation speed, a strong interaction of the space-time harmonics can be enabled; this results in the creation of a *directional* band-gap in one direction, while leaving propagation in the reverse direction intact [23]. The directional bandgap identifies a strong active parametric interaction [4], [5].

In the current article, we derive, based on the rigorous theoretical framework developed by Oliner et. al [4]–[6] and recently applied in the context of nonreciprocal media [21], [24], closed form expressions of important parameters that directly affect the non-reciprocity of modulated media. First, the bandgap width, for both forward and backward modulation is calculated. Second, the optimal range of the modulation speed is specified, which strongly depends on the trade-off between the modulation index and the speed of the modulation. We also report a closed form expression for the insertion loss and explicitly show the dependency on different system parameters. Although the analogy between space-time modulated media and scattering from crystalline structures had been discussed by Slater in an early work [9], the analysis carried out here exploit the metamaterial paradigm to establish the firm connection between space-time modulated media and inelastic Brillouin Scattering. Hence, we compute the complex refractive index, and harmonics wave impedances to show their behaviour whenever scattering occurs. Along the way, we examine the harmonic interactions from very low frequency values up to the bandgaps, both in the forward and backward directions. A geometrical description of a quantity that correlates with the strength of coupling with the space-time harmonics is constructed in the $k-\beta$ plane. The systematic analysis reveals a resonance like interaction due to a singularity in the secular equation. Finally, a detailed FDTD analysis is developed to verify and demonstrate the intriguing properties of space-time modulated media.

In section II a generalized dispersion relation is derived for an arbitrary space-time periodic medium. For subsequent discussions, the dispersion relation is simplified by considering the fundamental harmonic of the modulation wave only.

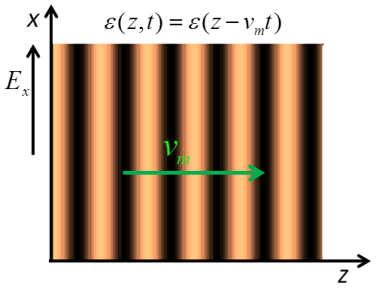

Fig. 1. A space-time modulated medium.

The analogy to Brillouin scattering is pointed out and the scattering centres are identified. Section III describes in detail the scattering mechanism in both the forward and backward propagation directions, the width of the bandgap as well as the insertion loss in the center of the gap are also estimated; the effect of the inelastic scattering on the extinction coefficient is also demonstrated. In section IV we provide a detailed FDTD analysis to verify the theoretical analysis.

II. Space-time Dispersion Relation

Here we will consider the case where the dielectric constant is modulated in both space and time as a travelling wave of the form $\epsilon(z,t)=\epsilon(z-\nu_m t)$, where ν_m is the modulation speed taken in the $+z$ direction. The analysis and derivations follow the rigorous treatment of early works by Oliner et. al and Cassedy [4]–[6], [25]. Due to its importance and relevancy to the current analysis, a detailed derivation of the dispersion relation is presented in this section. Not only is it necessary for nomenclature and completeness, but it also shows the intimate connection with Brillouin Scattering and forms the foundation for finding expressions which describe the nonreciprocal nature of the structure. ϵ can be expanded in terms of its Fourier harmonics

$$\epsilon=\epsilon_0\sum_{n=-\infty}^{\infty}\epsilon_n'\cos(n\omega_m t-n\beta_m z), \tag{1}$$

where ω_m and β_m are the temporal and spatial modulation frequencies, and are related to the modulation speed ν_m as:

$$\nu_m=\frac{\omega_m}{\beta_m}. \tag{2}$$

Seeking an x polarised TEM solution for the wave propagating along the z axis (Fig. 1), the wave equation can be written as

$$\frac{\partial^2 E_x(z,t)}{\partial z^2}=\mu_0\frac{\partial^2\epsilon(z,t)E_x(z,t)}{\partial t^2}. \tag{3}$$

The disturbance $\epsilon(z,t)$ in (3) is periodic in both time and space, hence we can apply Bloch-Floquet theorem to express the solution as a propagating wave $E_0\exp(-j[\omega t-\beta z])$ modulated by a space-time periodic function $P(\omega_m t-\beta_m z)$; where ω and β are the yet to be determined frequency and wave number. The periodic function P can in turn be written as an infinite Fourier series:

$$P(\omega_m t-\beta_m z)=\sum_{r=-\infty}^{\infty}a_r e^{-jr(\omega_m t-\beta_m z)}. \tag{4}$$

Therefore, the general solution assumes the form:

$$E_x(z,t) = \sum_{r=-\infty}^{\infty} a_r e^{-j[(\omega+r\omega_m)t-(\beta+r\beta_m)z]}, \quad (5)$$

where the arbitrary constant E_0 is absorbed in a_r [25]. Substituting (5) and (1) in (3); and noting that $\cos\theta = (\exp(j\theta)+\exp(-j\theta))/2$, a recursion relation between the a_r terms can be found to be

$$\sum_{s=1}^{\infty} \epsilon'_s \left(a_{r-s} + a_{r+s}\right) + F_r(k,\beta)a_r = 0, \quad r \in \mathbb{Z} \quad (6)$$

where

$$F_r(k,\beta) = 2\left(1 - \left[\frac{\beta a + 2\pi r}{ka + 2\pi\nu r}\right]^2\right), \quad (7)$$

$a = 2\pi/\beta_m$ the wavelength of the modulation, k is the unmodulated wave number ($k = \omega/c$), c is the speed of the unmodulated medium; and $\nu = \nu_m/c$ is the relative speed of the modulation. (6) represents an infinite system of linear algebraic equations that couple the r^{th} space-time (Floquet) mode to all other modes. To find the dispersion relation for a given k (β), a secular (or characteristic) equation is obtained by setting the determinant of the infinitely countable system (6) to zero; hence the corresponding β (k) can be calculated. When $v_m = 0$, $F_{-r}(k,-\beta) = F_r(k,\beta)$. Therefore the system of equations (6) is invariant under the reflection of r ($r \Rightarrow -r$), which means that if (k, β) is a solution to the characteristic equation so does (k, $-\beta$) and the modulated medium is reciprocal. However for a general $\nu_m \neq 0$, this is not the case and the medium is intrinsically non-reciprocal.

In practical situations, the expansion (1) can be truncated to the fundamental component (ω_m and β_m) only, which simplifies (6) to

$$a_{r+1} + D_r a_r + a_{r-1} = 0, \quad (8)$$

for $r \in \mathbb{Z}$ and

$$D_r = \frac{F_r(k,\beta)}{M} = \frac{2}{M}\left[1 - \left(\frac{\beta a + 2\pi r}{ka + 2\pi\nu r}\right)^2\right], \quad (9)$$

where $M = \epsilon'_1/\epsilon'_0$ is the modulation index [4]. The modulated media then couples the r^{th} Floquet mode with its nearest neighbour (+1 and -1 harmonics) only.

Formally, a rigorous *continued fractions* approach was derived to determine the dispersion relation [4], [5]. Expressing the ratio a_r/a_{r-1} as a continued fraction and noting that $a_r/a_{r-1} = (a_{r-1}/a_r)^{-1}$, the secular equation can be cast into the form of a continued fraction form [4], [5]

$$G_r(ka,\beta a) \equiv D_r - \cfrac{1}{D_{r-1} - \cfrac{1}{D_{r-2} - \cfrac{1}{\ddots}}} - \cfrac{1}{D_{r+1} - \cfrac{1}{D_{r+2} - \cfrac{1}{\ddots}}} = 0. \quad (10)$$

It is worth noting that $G_r(ka,\beta a) = G_0(ka + 2\pi\nu r, \beta a + 2\pi r)$, which means that the dispersion relation can be fully obtained from any of the infinite $G_r(ka,\beta a)$ and they are all compatible. Additionally, the relative amplitudes of the harmonics a_r can be written as a partial fraction [4], [11]

$$\frac{a_r}{a_{r-1}} = \cfrac{-1}{D_r - \cfrac{1}{D_{r+1} - \cfrac{1}{\ddots}}}. \quad (11)$$

The effect of D_r can be best understood by referring to (8); when D_r is significantly large (i.e, M is small), the rth harmonic vanishes. Therefore, the inverse of D_r indicates the strength at which a signal couples with its rth harmonic.

For infinitesimally small $M \to 0$, the equations (8) decouple and the dispersion relation reduces to

$$MD_r = 0 \Rightarrow \beta + r\beta_m = \pm\left(\omega + r\omega_m\right)/c, \quad (12)$$

the dispersion relation of the unmodulated medium, but shifted by $(r\beta_m, r\omega_m)$.

For each frequency ω, (10) determines the corresponding wave number β. Therefore, the dispersion relation can be constructed, which is generally a function of M and ν. However to guarantee that a_r/a_{r-1} converges for some $r > r_0$, it was shown that $|D_r|$ must be greater than 2; this is equivalent to saying that the modulation velocity v_m may not be very close to the speed c of waves in the unmodulated medium [4], [5]. Quantitatively ν may not be within the interval $\left[1/\sqrt{1+M^2},\ 1/\sqrt{1-M^2}\right]$. Moreover, for stable operation (all solutions bounded in time), the sub-sonic condition $\nu < 1/\sqrt{1+M^2}$ must be met. This enforces an upper bound on the modulation speed [6].

A. Connection to Brillouin Scattering

Equation (3) establishes the formal connection between space-time modulation and Brillouin Scattering. However the analogy between the two is deeply rooted and needs more discussion. Brilliouin Scattering (BS), whether Spontaneous or Stimulated, results from modulation of a crystal lattice electric permittivity. A spontaneous scattering process is responsible for light scattering, where the optical properties are unmodified by the presence of the incident light [7]. On the other hand, the optical properties depend on the incident light in a stimulated scattering process.

Spontaneous Brillouin Scattering stems from the inevitable fluctuation of thermodynamic variables, which affects the macroscopic properties of the crystal lattice. However such fluctuation is random, reciprocal and wide band [8]. Nevertheless, interaction is usually negligible except for a specific crystal mode: the one that satisfies the phase matching conditions [7], [8]. Additionally, the interaction is weak, with a very small relative speed $\nu \sim 1$ ppm.

On the other hand in a Stimulated Brillouin Scattering (SBS) process, the beating of an intense pump of frequency ω_p and probe (Stokes or Anti-Stokes) waves of frequency ω_S results in the enhancement of an acoustic wave of frequency $\Omega = \omega_p - \omega_S$, which in turn beats with the pump to reinforce the probe. The positive feedback process causes electrostriction in the optical medium. The process sustains since the three waves satisfy the phase matching condition [7].

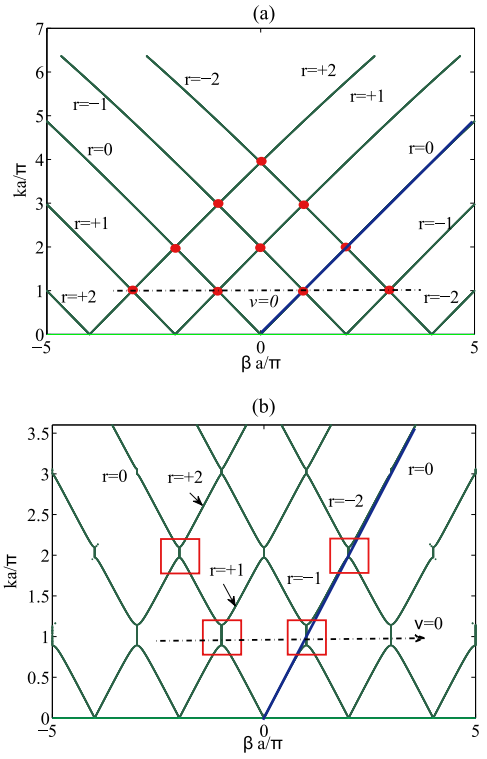

Fig. 2. Dispersion Characteristics for a space only modulated medium ($\nu = 0$) (a) negligibly small values of M. The forward fundamental branch $\omega = \beta c$ is highlighted. The dots represent the scattering centres where interactions are possible. Scattering centres in the forward (backward) direction correspond to Stokes (Anti-Stokes) centres. (b) $M = 0.5$; the forward fundamental branch $\omega = \beta c$ is highlighted. The rectangles identify the regions of strong harmonic scattering.

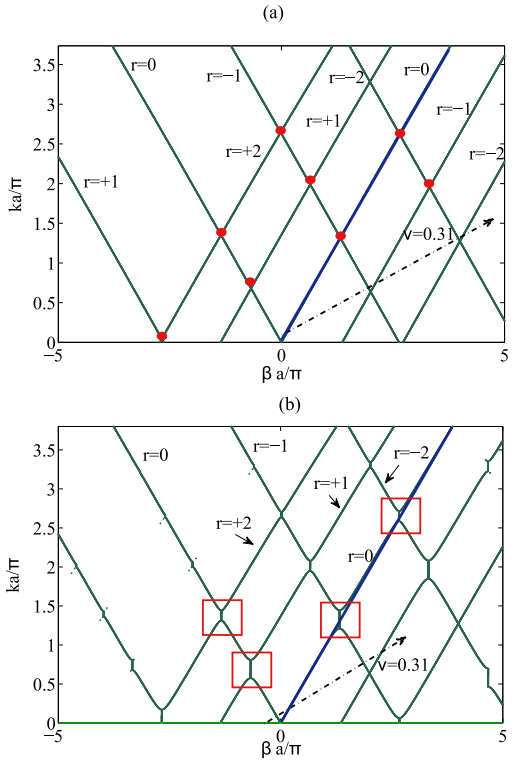

Fig. 3. Dispersion Characteristics for a space-time modulated medium ($\nu = 0.31$) (a) negligibly small values of M. The forward fundamental branch $\omega = \beta c$ is highlighted. The dots represent the scattering centres where interactions are possible. Scattering centres in the forward (backward) direction correspond to Stokes (Anti-Stokes) centres. (b) $M = 0.5$; the forward fundamental branch $\omega = \beta c$ is highlighted. The rectangles identify the regions of strong harmonic scattering.

In all cases, Brillouin Scattering results from the change of the permittivity in both space and time, which makes (3) applicable to such cases. Space-time modulated media can then be regarded as a *Stimulated* or *Engineered* Enhanced Brillouin Scattering. Such an analogue behaviour was recently exploited to describe the interaction of a longitudinal acoustic wave with a spatio-temporal phononic crystal [26].

B. Scattering Centres

For small values of M, the dispersion relation approaches (12). Figure 2(a) depicts the dispersion relation for a space only modulation medium ($\nu = 0$) and an infinitesimally small value of M. Comparing this to Fig. 2(b), which depicts the dispersion relation but for $M = 0.5$, (10), reveals that the intersection points between the $MD_r = 0$ lines identify the loci of strong interactions. As will be shown, for a general $\nu \neq 0$ these points allow the incident wave to scatter in an inelastic fashion and therefore will be called the *Scattering Centres*. The behaviour of such interactions can be studied by considering the interaction with the $r = 0$ branches only. In the forward direction ($\beta > 0$), the intersection point of the $r = 0$ branch and another arbitrary $r \neq 0$ branch can be found to be

$$k_r^F a = \beta_r^F a = r\pi\,(1+\nu) \quad \text{for } r < 0, \tag{13}$$

where the subscript r identifies that this is the intersection with the r^{th} branch and the superscript F emphasises that this is for a forward propagating wave (along $+z$ axis). Similarly k_r^B and β_r^B, the intersection with the backward branch is found to be

$$k_r^B a = -\beta_r^B a = r\pi\,(1-\nu) \quad \text{for } r > 0. \tag{14}$$

For reasons that will be revealed in Section III, we call the forward and backward scattering centres Stokes' and Anti Stokes' centres, respectively. For a forward propagating modulation, $\nu \geq 0$ and hence $k_r^B \leq k_r^F$; the equality holds for $\nu = 0$: space only modulated medium. The inequality $k_r^B < k_r^F$ means that the interaction in the backward branch occurs at a lower frequency leading the medium to become non-reciprocal. Fig. 3 presents the dispersion relation for $\nu = 0.31$ and two values of M: $M = 0$ and $M = 0.5$. It is clear that $k_r^B < k_r^F$.

It is worth noting that for a given frequency, there is an infinite number of wave numbers, identifying possible modes of propagation. Hence a complete solution is the linear superposition of all such modes. However for small M values, the first and second branches ($r = 0, \pm 1$) have the most significant contribution. As will be seen in Section III away from the scattering centres, only the first branch needs to be considered. In the vicinity of the scattering centres, both the first and second branches play a significant role.

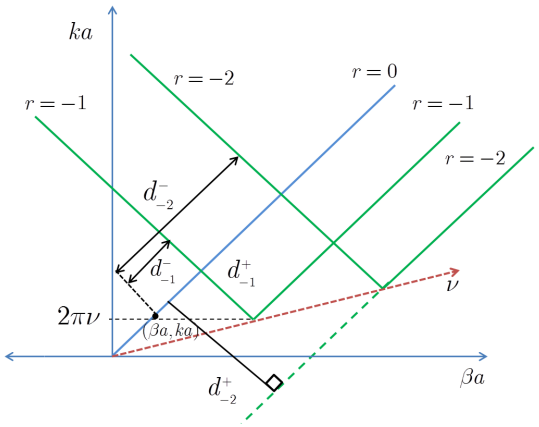

Fig. 4. Geometrical Description of the dispersion characteristics.

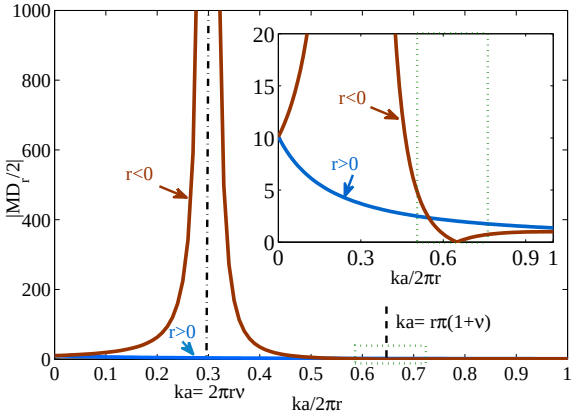

Fig. 5. Normalized D_r as a function of the normalized frequency ka for the forward propagation.

III. Scattering Mechanism

In this section we describe the conversion (scattering) process from the fundamental wave with frequency ω and wave number β to its space-time harmonics with frequency $\omega+r\omega_m$ and wave number $\beta+r\beta_m$. The scattering behaviour depends on the values of D_r. First, we examine the trend of D_r as a function of the input frequency ω or the corresponding scaled value ka. Toward this end, D_r is related to metric distances on the $ka-\beta a$ plane. Referring to Fig. 4, the distances d_r^+, between an arbitrary point $(\beta a, ka)$ on the $r=0$ line and the branch of $D_r=0,\ r\neq 0$ with a positive slope is

$$d_r^+ = \frac{|(\beta a + 2\pi r) - (ka + 2\pi\nu r)|}{\sqrt{2}} = \frac{2\pi|r|(1-\nu)}{\sqrt{2}}, \quad (15)$$

which is obtained by substituting the coordinate $(\beta a = ka, ka)$ in the expression $ka+2\pi\nu r-\beta a-2\pi r$ and dividing by $\sqrt{2}$. Similarly, the distance d_r^- between $(\beta a, ka)$ and the branch of $D_r=0$ with a negative slope $(ka+2\pi\nu r=-(\beta a+2\pi r))$ is

$$d_r^- = \frac{|(\beta a + 2\pi r) + (ka + 2\pi\nu r)|}{\sqrt{2}}. \quad (16)$$

Therefore,

$$M|D_r| = \frac{4 d_r^+ d_r^-}{(ka+2\pi r\nu)^2}. \quad (17)$$

The above Eq., together with Fig. 4, give a pictorial view of how $|D_r|$ depends on the geometrical metrics d_r^+ and d_r^-. It is worth noting that the metric distances d_r^- and d_r^+ as well as the derived expression of $|D_r|$ are only valid for small values of M and at points sufficiently away from the bandgaps, highlighted in Figs. 2(b) and 3(b), such that the dispersion relation$\beta a = ka$ is valid. Nevertheless, the general behaviour of D_r around the bandgaps can still be described using the $\beta a = ka$ approximation; for accurate results we resort to the general secular equation (10). For very small values of βa and ka, $|D_r| = 2/M(1-\nu^2)/\nu^2$ and is independent of r; this means that for very low frequencies all $|D_r|$ basically have the same value. Nevertheless as ka increases, D_r effect is radically different for waves travelling in the forward or backward directions, as will be detailed in the next two subsections.

A. Forward direction ($\beta > 0$)

For a wave travelling in the $+z$ direction and assuming that propagation is mainly due to the $r=0$ branch, $\beta a = ka$. Fig. 5 shows the change of D_r as a function of the normalized frequency $ka/2\pi r$. For $r<0$ ($r>0$), as ka increases along the $r=0$ line, d_r^- linearly decreases (increases) and d_r^+ remains constant (refer to Fig. 4). Additionally, the denominator of (17) quadratically decreases (increases). Therefore, for $r>0$, the net effect of both terms keeps $|D_r|$ monotonically decreasing.

The trend of $|D_r|$ for $r<0$ is more dynamic; as ka approaches the singularity at $-2\pi r\nu$, $|D_r|$ increases without bound. However, as ka increases further, $|D_r|$ will decrease and eventually vanish at the Stokes' centre $ka = r\pi(1+\nu)$. At this point the r^{th} branch intersects the main branch (i.e, $d_r^- = 0$) and the interaction is the strongest, as was already shown in Figs. 2 and 3. For such cases where $|D_r|$ attains small values, the continued fraction in (10) has to be used to determine βa. Otherwise, the dispersion characteristic is determined via $D_0 = 0$ alone, which is equivalent to the approximation used here ($ka = \beta a$). The singularity corresponds to higher harmonic generation, where the wave interacts with its higher harmonics only. However, this interaction is passive and weak(for a detailed analysis, please refer to Appendix A.)

On the other hand, the interaction at $ka = r\pi(1+\nu)$ between the fundamental and its $-|r|$ harmonic is much stronger. In general the first interaction (with the -1 harmonic) is the strongest and provides the wider bandwidth. For this reason and because it is straight forward to find closed form expressions, we will restrict our attention to the -1 harmonic interaction. At $ka = r\pi(1+\nu)$, D_{-1} is small (inset of Fig. 5) to the extent that the dispersion relation (10) can be truncated to

$$D_0 D_{-1} - 1 = 0 \quad (18)$$

Letting $\beta a = ka + \eta = \pi(1+\nu) + \eta$, where $|\eta| \ll \pi(1+\nu)$, η can be approximated to

$$\eta = \pm j\pi(1-\nu^2)^{1/2} M/4. \quad (19)$$

In terms of the wave number

$$\beta = k\left(1 \pm j\alpha_F\right), \quad (20)$$

where

$$\alpha_F = \frac{M}{4}\sqrt{1-\frac{\omega_m}{\omega}} = \frac{M}{4}\sqrt{\frac{1-\nu}{1+\nu}}. \tag{21}$$

Unlike (51), η is imaginary and first order in M, indicating a strong active interaction [27]. The amplitude of the -1 harmonic can be found to be

$$\frac{a_{-1}}{a_0} = -D_0 = \pm j\sqrt{\frac{1-\nu}{1+\nu}} \equiv \pm jb, \tag{22}$$

which, unlike (52), does not depend on M.

Inside the bandgap the $r=-1$ branch has a significant contribution to the total solution. Hence, the general solution can be written as follows [3]

$$E_x = a_+ E_{x+} + a_- E_{x-}, \tag{23}$$

where

$$E_{x\pm} = \left(e^{-j(\omega t - kz)} \pm jbe^{-j([\omega-\omega_m]t-[k-\beta_m]z)}\right) e^{\pm\alpha_F kz}, \tag{24}$$

Please note that the above general solution assumes that the contributions from other branches are ignored (ignoring the multi-valued character of $k(\omega)$). Noting that [3]

$$\frac{\omega}{k} = -\frac{\omega-\omega_m}{k-\beta_m}, \tag{25}$$

the characteristic impedances of the space-time medium at frequencies ω and $\omega-\omega_m$ are

$$Z_0 = \frac{\bar{Z}}{1 \mp j\alpha_F} \tag{26}$$

and

$$Z_1 = \frac{-\bar{Z}}{1 \pm j\alpha_F/\left(1-\omega_m/\omega\right)}, \tag{27}$$

respectively, and $\bar{Z} = \omega\mu_0/k$ is the impedance of the unmodulated medium.

According to (25), the fundamental and scattered waves have phase velocities which are equal in magnitude but opposite in direction. Moreover, the sign of Z_1 is negative implying that the scattered wave is travelling in the $-z$ direction. This is consistent with Coupled Mode Theory predictions where active interaction is possible between waves which have the same magnitude of phase velocity and energy flow is contradirective [28]. Additionally, the phase matching conditions automatically emerge:

$$\omega_S = \omega - \omega_m \tag{28}$$

$$\beta_S = \beta - \beta_m. \tag{29}$$

Since the scattered wave is red-shifted (lower in frequency), it corresponds to a Stokes' wave, which explains why the scattering centre was named Stokes' centre earlier in Section II.

Considering the situation depicted in Fig. 6, where a wave of frequency ω impinges the modulated medium of length d. The tangential fields E_x and H_y are continuous at the interfaces $z=0$ and $z=d$. Approximating the impedance of the fundamental and +1 harmonic to $\bar{Z}$ and $-\bar{Z}$, respectively

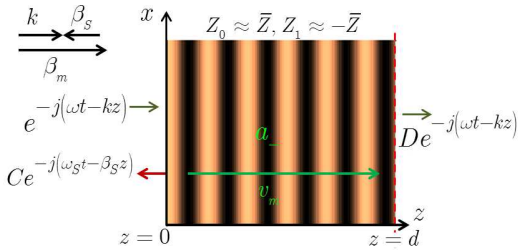

Fig. 6. Simplified boundary value problem for an incident wave that is co-directional with the modulation wave.

as shown in the Fig., the amplitude D of the transmitted wave is found to be

$$D = e^{-\alpha_F k_0 d} \tag{30}$$

and the Insertion Loss, IL, of the modulated medium in dB is

$$\text{IL} = 20\log(\alpha_F kd) = 8.686\frac{\pi}{4}M\sqrt{1-\nu^2}\frac{d}{a}, \tag{31}$$

which reveals interesting conclusions. As expected the attenuation is directly proportional to M, but decreases as the modulation speed ν_m increases. It is then desirable to make ν_m as small as possible. However, as will be shown in the subsection C, ν_m has a lower bound determined by non-reciprocity. Additionally, from (31) the attenuation is proportional to the normalized length of the medium (normalized to the modulation wavelength); hence suggesting that to have an efficient scattering the modulation wavelength a should be as small as possible. However, this might be constrained by the lower or upper bound of ν_m.

B. Backward Direction ($\beta < 0$)

For the backward propagation $\beta<0$, the D_r values along the $\beta a = -ka$ line assume the form

$$\left|\frac{MD_r}{2}\right| = \left|1-\left(\frac{1-ka/2\pi r}{\nu+ka/2\pi r}\right)^2\right|. \tag{32}$$

Fig. 7 shows how D_r changes as a function of the input frequency. Although the D_r trend in Fig. 7 look similar to Fig. 5, there are some fundamental differences which do not allow the backward propagation to be treated as the mere dual of the forward one. First, for the forward propagation, at the singularity $ka=2\pi\nu$ the interaction is with the $r>0$ harmonics only. As a result, it was shown in the previous subsection that the +1 harmonic interacts passively with the fundamental. Additionally, it is not possible to position the singularity at the Stokes' scattering centre $ka=\pi(1+\nu)$. However for backward propagation, the singularity is still at $ka=2\pi\nu$. Additionally, choosing $\nu=1/3$ positions the singularity at the Anti-Stokes' centre, hence limiting the scattering to be strictly with the $r>0$ harmonics only; in other words, power is converted to the higher harmonics only (up conversion). (c.f. Appendix A for more details on higher harmonic generation). Similar to the analysis of the previous subsection, the truncated secular equation

$$D_0 D_{-1} - 1 = 0 \tag{33}$$

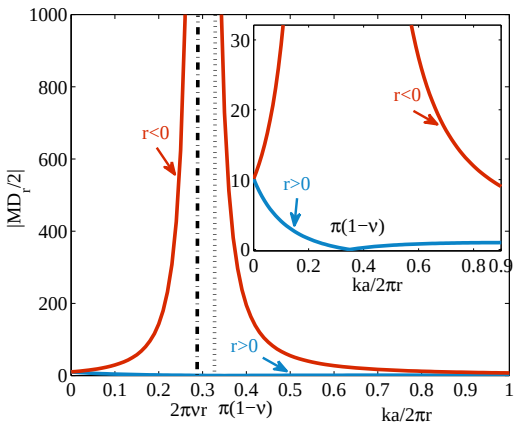

Fig. 7. Normalized D_r as a function of the normalized frequency ka for the backward propagation.

can be solved to find the propagation constant $\beta a = -ka + \eta$ at $ka = \pi(1-\nu)$. Neglecting terms of order higher than η^2, η is found to be

$$\eta = \pm j\pi \left(1-\nu^2\right)^{1/2} \frac{M}{4}, \tag{34}$$

identical to (19). In terms of the wave numbers

$$k = k_0 \left(1 \pm j\alpha_B\right), \tag{35}$$

where

$$\alpha_B = \frac{M}{4}\sqrt{1+\frac{\omega_m}{\omega}}. \tag{36}$$

Similarly,

$$\frac{a_1}{a_0} = \pm j\sqrt{\frac{1+\nu}{1-\nu}} \equiv \pm jb \tag{37}$$

For small values of M, Fig. 8 shows the situation where the modulated medium is impinged by a wave at frequency ω. It is worth to notice that the two situations depicted in Figs. 6 and 8 represent waves which have different frequencies. In the forward direction the wave is at a normalized frequency $\pi(1+\nu)$, while in the backward direction its normalized frequency is $\pi(1-\nu)$.

The backward IL takes a form identical to (31), but at a normalized frequency of $ka = \pi(1-\nu)$. This means that by the proper selection of M and ν the medium acts as non-reciprocal bandstop filter, where the forward and backward stop bands can occur at different frequency ranges.

The scattered wave is an Anti-Stokes wave and the interaction automatically satisfies the phase matching conditions

$$\omega_A = \omega + \omega_m \tag{38}$$
$$\beta_A = \beta + \beta_m. \tag{39}$$

The r^{th} harmonic impedance Z_r can be expressed in terms of the normalized frequencies and wave numbers as

$$Z_r = \bar{Z}\frac{ka + 2\pi\nu r}{\beta a + 2\pi r}. \tag{40}$$

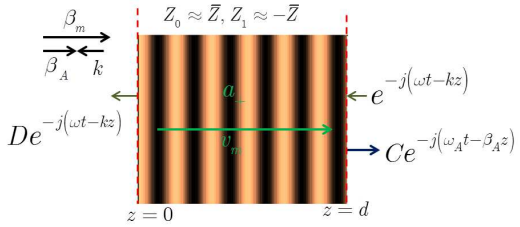

Fig. 8. Simplified boundary value problem for an incident wave travelling in a direction opposite to the modulation.

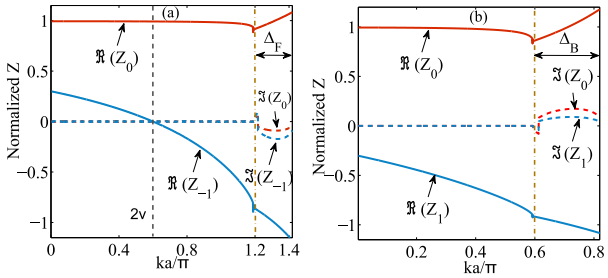

Fig. 9. The harmonic impedance versus frequency: (a) Forward modulation, (b) Backward modulation.

Fig. 9 presents the Z_r for the fundamental and the first harmonic calculated up to the first bandgap. For the forward modulation, it is clear that the Z_{-1} vanishes when $ka = 2\pi\nu$, corresponding to the modulation frequency ω_m and the singularity discussed in subsection III-A and Appendix A. The vanishing of impedance re-confirms that no power is scattered to the lower harmonics at the singularity. For forward (backward) case, the impedance of the Stokes' (Anti-Stokes') harmonic is close to $\bar{Z}$ in the bandgap. Assuming that the unmodulated medium is matched to the input and output regions, the modulated medium is reasonably matched inside the bandgap. Additionally, the negative sign of the Stoke's and Anti-Stokes' impedances signify the back scattering of the harmonics.

The analysis leading to (37) and (37) for the forward and backward directions, respectively assumed that interactions with harmonics other than the first ones are insignificant and can be ignored. To show this, the relative amplitudes given by (11) are determined as depicted in Fig. 10. For frequencies below the first bandgap (in the highlighted areas), all harmonics have small amplitudes. Inside the bandgaps only the $r = -1$ ($r = +1$) harmonic has a significant value for the forward (backward) case, justifying the previous analysis. Inside the second bandgap ($ka \approx 2.5\pi$: forward, $ka \approx 1.5\pi$: backward), the second harmonic has a significant amplitude with a considerably large first harmonic amplitude.

C. Width of Directional Bandgap

The width of the directional bandgap determines the bandwidth at which the medium exhibits strong non-reciprocity. It also sets the lower bound on the modulation speed ν. To demonstrate non-reciprocity in one direction only, the forward

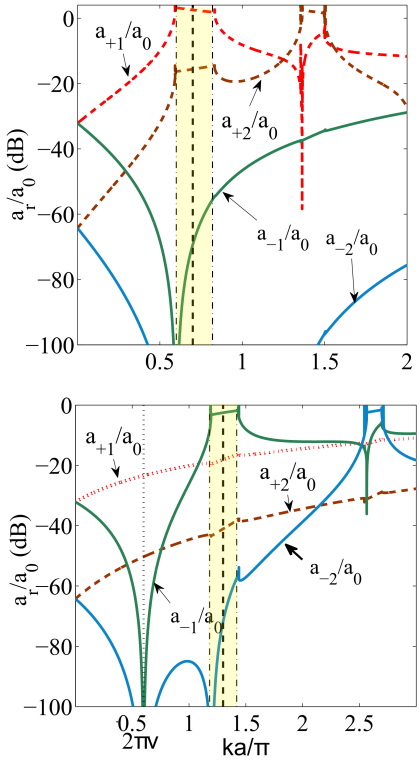

Fig. 10. The amplitude of the first few harmonics, $r = \pm 1, \pm 2$ for $M = 0.5, \nu = 0.3$. Bottom: Forward modulation. Top: Backward modulation.

and backward bandgaps must not overlap. Hence

$$\frac{\Delta_F + \Delta_B}{2} < 2\pi\nu, \tag{41}$$

where Δ_F and Δ_B are the directional bandgaps in the forward and backward directions, respectively. At the band edges $\beta a = \pi(1 \pm \nu)$ (Fig. 11). Substituting these values in the corresponding secular equations (18) and (33), it can be found that to second order:

$$\Delta_F = \Delta_B = \pi \left(1 - \nu^2\right)^{1/2} \frac{M}{2}. \tag{42}$$

Therefore, the minimum value of ν is determined from the inequality (41) to be

$$\nu_{\min} = M/4, \tag{43}$$

which is identical to the value determined in [23] for modulated elastic media. Therefore for optimum non-reciprocal behaviour

$$\frac{M}{4} < \nu < 1/\sqrt{1 + M^2}, \tag{44}$$

the upper bound is enforced by the necessity that of convergence $|D_r| > 2$ [4]. On one side it is desirable to increase M to increase the IL as given by (31). However on the other side, this decreases the range of possible values that the modulation speed ν_m can attain.

D. Complex Refractive Index, $\tilde{n} = n + j\kappa$

At an arbitrary incident frequency ω, the complex wavevector $\tilde{k}$ can be written as

$$\tilde{k} = \tilde{n}k, \tag{45}$$

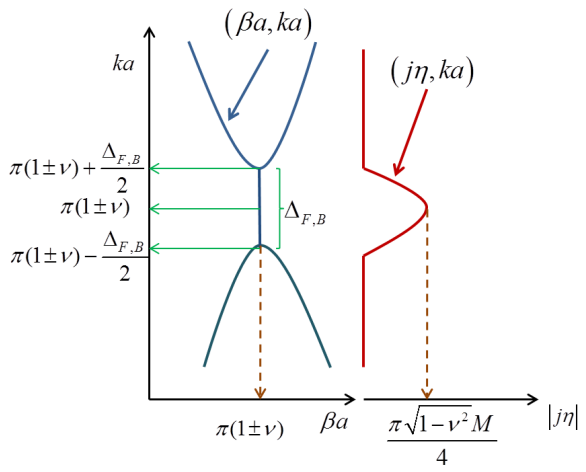

Fig. 11. Normalized frequency versus propagation and attenuation constants at the vicinity of the bandgap.

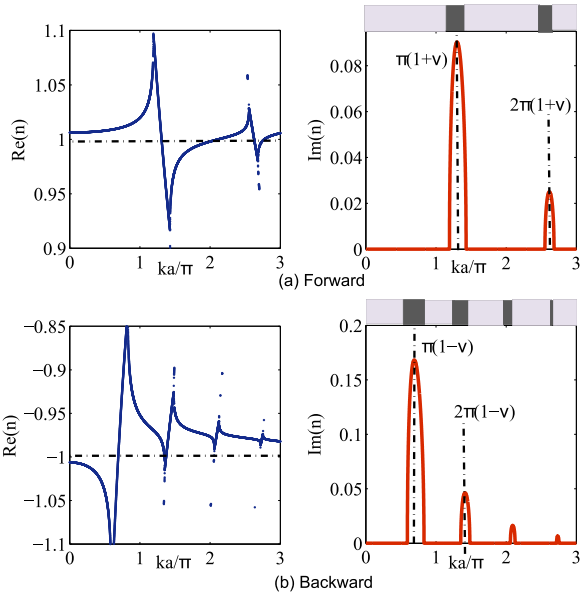

Fig. 12. Refractive index and extinction coefficient of waves having normalized frequency ka. (a: Forward direction. (b): Backward direction (the real part of the refraction coefficient is negative to emphasize that the wave is travelling in the $-z$ direction). The dark and bright bands on top of the extinction coefficient plots depict the situations when the medium is opaque or transparent, respectively.

where $\tilde{n} = n + j\kappa$ is the complex refractive index. The imaginary part determines the efficiency of the power scattered by the space-time harmonics (forward: $\omega - \omega_m$, backward $\omega + \omega_m$). Using the dispersion relation (10), the refractive index is calculated for the forward and backward directions as shown in Fig. 12. For the calculations, 20 terms were used to compute the continued fractions; usually four of five terms are enough, as the continued fractions rapidly converge.

From Fig. 12, it is clear that the optical property of the medium is non-reciprocal; absorption occurs at different input frequencies. Additionally, the widths of the Stokes and Anti Stokes Centres are basically the same because $\Delta_F = \Delta_B$ as was already determined in the previous subsection.

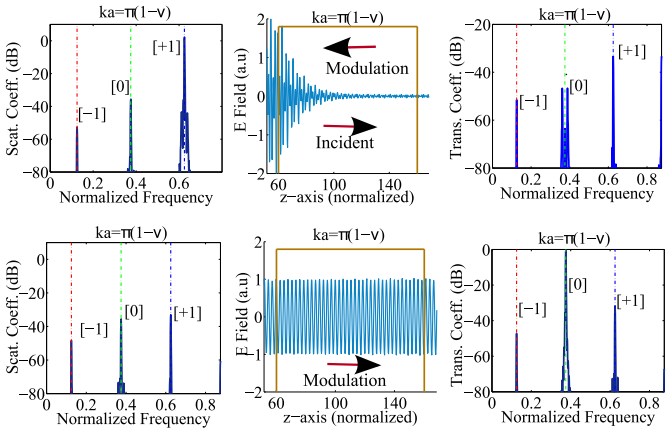

Fig. 13. FDTD simulated spectra for the scattered and transmitted waves for $\pi(1-\nu)$. The modulation speed changed direction and the system exhibits a non-reciprocal behaviour. ([0]: incident wave at ω, [-1]: $\omega-\omega_m$, [+1]: $\omega+\omega_m$).

IV. FDTD Analysis

To validate the theoretical findings and provide deeper insight on the non-reciprocal behaviour of space-time modulated media, FDTD was applied to the 1D problem. The space-time dependence of the permittivity was used to modify the update equations of the FDTD formalism to determine the propagation and scattering behaviour of a space-time modulated medium. For more details on the FDTD implementation please refer to Appendix B. Fig. 13(a) presents the scenario where $ka=\pi(1-\nu)$ and the modulation travels in the $-z$ direction, In this case, the incident wave interacts with its +1 harmonic, which scatters energy back in the $-z$ direction, as is clear after inspecting the frequency spectrum of the scattered field. At this point, the scattered wave is the Anti-Stokes' wave in Brillouin Scattering. However if the modulation speed was inverted as in Fig. 13(b), the modulation and incident waves are co-directional. In this case, as shown in Fig. 13(b), propagation is not disturbed and the medium is transparent. Hence, the medium is non-reciprocal at $ka=\pi(1-\nu)$, in agreement with the analytical predictions.

To demonstrate that scattering occurs only inside the band gap, Fig. 14 depicts three different situations, where the FDTD algorithm was used to determine the wave propagation behaviour for an input wave of $ka=0.8\pi(1-\nu)$, $ka=\pi(1-\nu)$ and $ka=1.2\pi(1-\nu)$, when $M=0.1$ and $\nu=0.1$. The first and last frequencies are outside the bandgap. As expected, strong Brillouin-like scattering occurs when $ka=\pi(1-\nu)$ only, as can be seen by the amplitude of the scattered wave at $\omega+\omega_m$. For the other two out-of-band frequencies ($ka=0.8\pi(1-\nu)$ and $ka=1.2\pi(1-\nu)$) the medium is transparent, demonstrated by 0 dB in the transmission spectra in Figs. 14(a) and (c).

According to Eqs. 36 and 35, the field at ω is actively converted to the one at $\omega_A=\omega+\omega_m$. To demonstrate this, Fig. 15 presents the fields calculated at both frequencies. These plots are determined from the FDTD computations, after applying Fourier transform. The plots do indeed verify that the conversion is exponential; the incident fields are scattered

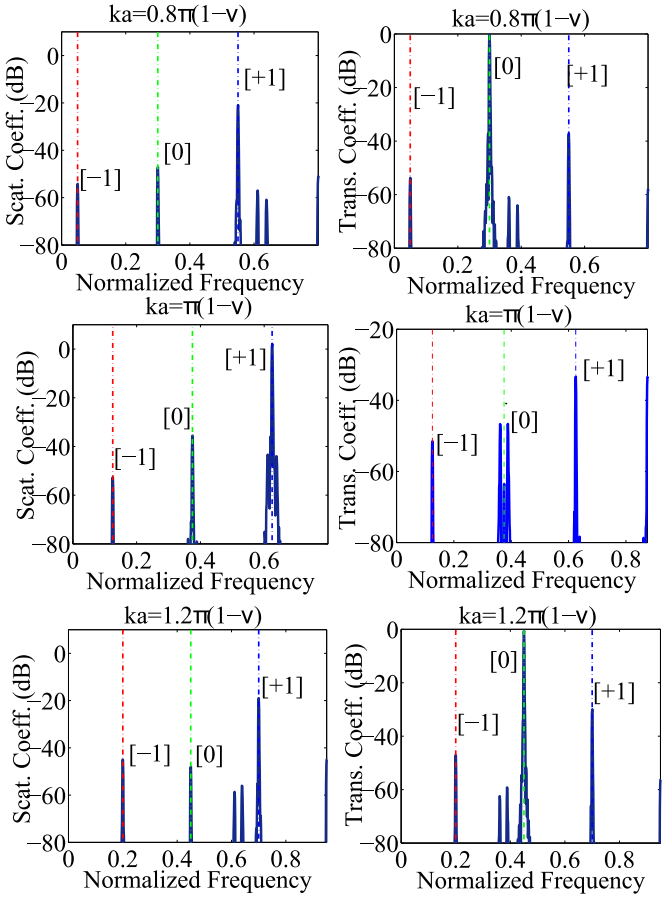

Fig. 14. FDTD simulated spectra for the scattered and transmitted waves for $0.8\pi(1-\nu)$, $\pi(1-\nu)$ and $1.2\pi(1-\nu)$. ([0]: incident wave at ω, [-1]: $\omega-\omega_m$, [+1]: $\omega+\omega_m$).

into the $\omega+\omega_m$ frequency (blue-shifted), which bounces back to the source. Additionally, the envelopes of the two waves, determined from (36), (35) and (37) match the FDTD calculations.

Equation (31) predicts that not only does the insertion loss, IL, per unit length is controllable by M, it also can be controlled by varying the modulation wavelength. If the modulation wavelength was made much smaller than the slab thickness, significant IL can be obtained. The controllability through the wavelength can obviously compensate for the limitation on M as given by the optimal range (44). In Fig. 16 the insertion loss normalized to the slab thickness d is calculated using (31) and FDTD. Insertion losses of values above 40 to 50 dB cannot be accurately determined via the amplitude at the output side of the signal component due to the limited dynamic range of the FDTD method [29]. In the Fig. the IL using the values at the output side saturates at around 50 dB. Therefore, the IL was calculated from the FDTD data via the slope of the local maxima and minima, which can be fitted to an exponential curve. From Fig. 16, it is clear that (31) accurately predicts the IL values. Additionally from (31), the modulation speed does not significantly affect the IL. In fact changing ν from 0.1 to 0.2 and 0.3, while keeping other parameters appearing in (31) fixed, results in a decrease

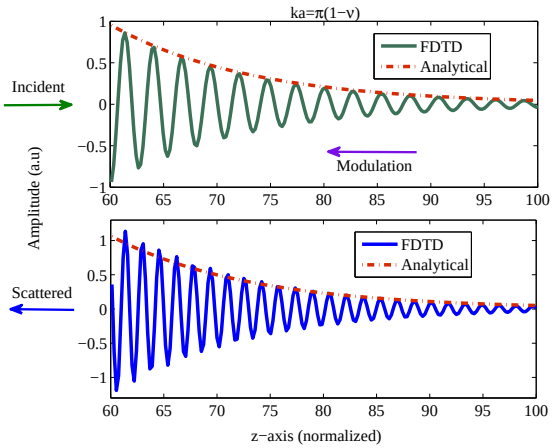

Fig. 15. Electric field inside the active (modulated) region for frequency component $ka = \pi(1-\nu)$ and the +1 harmonic, showing exponential conversion.

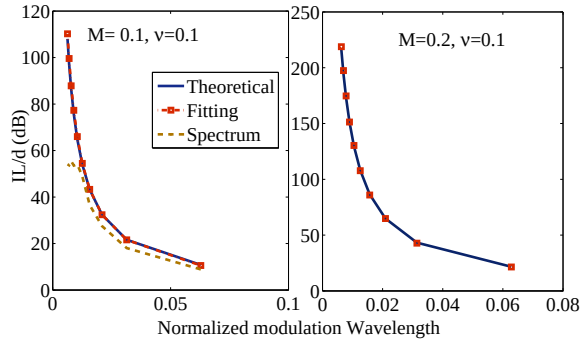

Fig. 16. The insertion loss (IL), normalized to the modulated slab thickness, calculated form $M = 0.1$ and $M = 0.2$.

of IL by 1.33% and 4%, respectively. These reductions are consistent with the theoretical prediction based on (31) (1.52% and 4.1%).

The modulation wavelength can be possibly controlled using the Distributedly Modulated Capacitance (DMC) technique [19]. In this case, the dispersion characteristic of the carrier transmission line can be engineered to achieve some specific wavelengths that specify the modulation wavelength on another coupled transmission line.

As discussed earlier, the modulation results in a bandgap, where scattering is the strongest at the centre of the gap and decreases until it eventually becomes zero at the band edges. In Fig. 17 we plot the FDTD calculated insertion loss for different input frequencies inside the gap, superimposed on the dispersion characteristics determined by (10). As Fig. 17 shows, the insertion loss is maximum at the centre of the bandgap and becomes negligibly small at the band edges.

V. Conclusion

A systematic analysis of the harmonics interactions present in a space-time modulated medium is carried out over a frequency range which extends from DC up to around the bandgaps in both the forward and backward directions. It is

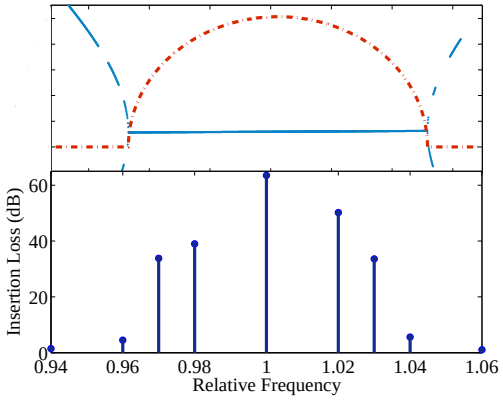

Fig. 17. FDTD simulated insertion loss for different frequencies in the vicinity of the band gap, superimposed on the calculated dispersion relation near the band gap.

demonstrated that a passive second harmonic generation process does occur due to the singularity in the secular equation. However such behaviour is very weak and can be ignored. On the other hand, bandgaps in the forward and backward directions are created due to the active parametric interaction of an incident wave with its space-time harmonics. In this regime, the interaction can be described using a Brilliouin-like scattering process. The strength of scattering from a bandgap as well as its width were determined. To have an optimal full non-reciprocal behaviour, the modulation speed may not be below a certain threshold which is a function of the modulation index. Finally FDTD was used to verify the theoretical results and findings.

Appendix A: Behaviour at the Singularity $ka = 2\pi\nu r$

At the first singular point $ka = 2\pi\nu$, the secular equation (10) reduces to

$$D_0 - \cfrac{1}{D_{+1} - \cfrac{1}{D_{+2} - \cfrac{1}{\ddots}}} = 0, \tag{46}$$

i.e, it depends on the interaction between the main branch and the positive r space time harmonics. To find the properties and strength of this interaction, it is assumed that at $ka = 2\pi\nu$, D_r for $r > 1$ are large enough such that their contribution to the secular equation can be ignored. This is consistent with the monotonically decreasing trend of $|D_r|$, $r > 0$ (Fig. 5). One can then solve the truncated equation:

$$D_0 D_{+1} - 1 = 0 \tag{47}$$

to find βa, evaluated at $ka = 2\pi\nu$. Since βa is not very different from its value at $r = 0$, it can be approximated by

$$\beta a = 2\pi\nu + \eta, \quad |\eta| \ll 1. \tag{48}$$

Neglecting orders in η higher than two, the truncated characteristic equation (47) is reduced to

$$\eta^2 \left[\frac{\gamma^2 - 1}{(2\pi\nu)^2} + \frac{2\gamma}{(2\pi\nu)^2} \right] + \eta \frac{\gamma^2 - 1}{\pi\nu} - \left(\frac{M}{2} \right)^2 = 0, \tag{49}$$

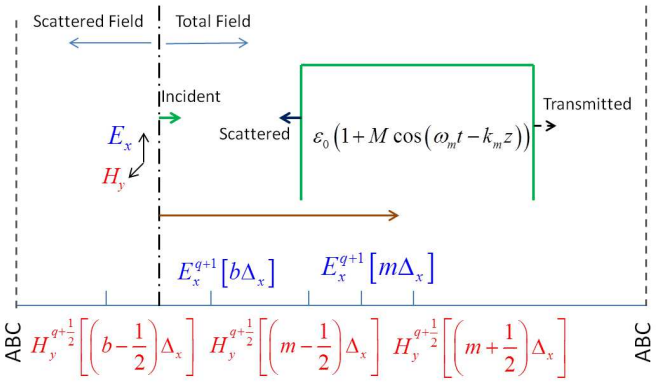

Fig. 18. Grid used for the FDTD solver. The space-time modulated media is excited by an incident plane wave introduced at the TF/SF interface.

where $\gamma = (\nu+1)/2\nu$ and is always greater than one (since $\nu < 1$). The type of the solution is determined by the radical, which for the case in hand, is always positive. Hence, η is real, indicating a passive exchange of power between the wave at normalized frequency $ka = 2\pi\nu$ and its space-time harmonic $ka + 2\pi\nu = 2ka$ [27]. This interaction corresponds to a weak second harmonic generation. To estimate the magnitude of the interaction (i.e, finding η), one notices that for $\eta^2 \ll |\eta|$

$$\eta \approx \frac{\pi\nu^3 M^2}{1+2\nu-3\nu^2}, \tag{50}$$

a second order in M. Therefore

$$\beta a \approx 2\pi\nu\left(1+\frac{M^2\nu^2}{2\left(1+2\nu-3\nu^2\right)}\right). \tag{51}$$

The ratio of the amplitude of the +1 harmonic and the fundamental can be determined as

$$\frac{a_1}{a_0} = -D_0 \approx \frac{2M\nu^2}{1+2\nu-3\nu^2}. \tag{52}$$

Substituting with the typical values, $M = 0.5$, $\nu = 0.3$, $a_1/a_0 \approx 0.07$, a very small number. Therefore, it can be concluded the the interaction between the fundamental and its +1 harmonic is very weak and can be neglected in the cases of interest. This conclusion is consistent with the dispersion relations plotted in Figs. 2(b) and 3(b), where at $ka = 2\pi\nu$, the dispersion relation is basically that of the unmodulated medium.

Appendix B: FDTD Implementation

As depicted in Fig. 18, the medium is excited by an incident wave travelling in the $+z$ direction, which is applied at a Total Field/Scattered Field (TF/SF) interface [30], [31]. To the right of the interface is the total field region. The grid is terminated from both sides by absorbing boundaries. The electric and magnetic fields are polarized in the x and y directions, respectively to guarantee that the wave propagates in the $+z$ direction. Taking into account the space time variation of the dielectric constant ϵ, the FDTD discretized form of Ampere's law can be written in terms of Courant number $S_c \equiv c\Delta_t/\Delta_z$ (where Δ_z and Δ_t are the discretized spatial and temporal step, respectively) as:

$$(E_x)_m^{q+1} = \frac{\epsilon_m^q}{\epsilon_m^{q+1}}(E_x)_m^q - \frac{\eta_0 S_c}{\epsilon_m^{q+1}}\left((H_y)_{m+1/2}^{q+1/2} - (H_y)_{m-1/2}^{q+1/2}\right).$$

Here the superscript and subscript indicate the time and spatial steps, respectively; η_0 is the impedance of free space, and ϵ_m^q is the relative permittivity at grid point m at time $q\Delta_t$. The update equation of the magnetic field is obtained via the discretization of Faraday's law:

$$(H_y)_{m+1/2}^{q+1/2} = (H_y)_{m+1/2}^{q-1/2} - \frac{S_c}{\eta_0}\left((E_x)_{m+1}^q - (E_x)_m^q\right).$$

The TF/SF plane is positioned between an H and E nodes. Hence the update equation for the H node at $b-1/2$ and E node at b are amended by the following equations [30]

$$(H_y)_{b-1/2}^{q+1/2} = (H_y)_{b-1/2}^{q+1/2} + \frac{S_c}{\eta_0}E_{ox}^{\text{inc}}\cos(\omega q\Delta_t)$$

$$(E_x)_b^{q+1} = (E_x)_b^{q+1} + \frac{S_c}{\epsilon_b^{q+1}}E_{ox}^{\text{inc}}\cos(\omega(q+1/2)\Delta_t + k\Delta x_2),$$

where E_{ox}^{inc} is the electric field of the incident wave, ω and k are its frequency and wave number, respectively. In the above eqns., the incident electric field is referenced to the position $b\Delta_z$ (i.e, $E = E_{ox}^{\text{inc}}\cos(\omega t - k[z-b])$).

References

[1] P. Tien, "Parametric amplification and frequency mixing in propagating circuits," *Journal of Applied Physics*, vol. 29, no. 9, pp. 1347–1357, 1958.
[2] A. Cullen, "A travelling-wave parametric amplifier," *Nature*, vol. 181, no. 4605, pp. 332–332, 1958.
[3] J.-C. Simon, "Action of a progressive disturbance on a guided electromagnetic wave," *IRE Transactions on Microwave Theory and Techniques*, vol. 8, no. 1, pp. 18–29, 1960.
[4] A. A. Oliner and A. Hessel, "Wave propagation in a medium with a progressive sinusoidal disturbance," *IRE Transactions on Microwave Theory and Techniques*, vol. 9, no. 4, pp. 337–343, July 1961.
[5] E. S. Cassedy and A. A. Oliner, "Dispersion relations in time-space periodic media: Part i; stable interactions," *Proceedings of the IEEE*, vol. 51, no. 10, pp. 1342–1359, Oct 1963.
[6] E. S. Cassedy, "Dispersion relations in time-space periodic media part ii; unstable interactions," *Proceedings of the IEEE*, vol. 55, no. 7, pp. 1154–1168, July 1967.
[7] R. W. Boyd, *Nonlinear optics*, 3rd ed. Boston: Boston : Academic Press, 2008.
[8] I. L. Fabelinskii, *Molecular scattering of light*. Springer Science & Business Media, 2012.
[9] J. C. Slater, "Interaction of waves in crystals," *Reviews of Modern Physics*, vol. 30, no. 1, p. 197, 1958.
[10] S. Y. Elnaggar and G. N. Milford, "Description and stability analysis of nonlinear transmission line type metamaterials using nonlinear dynamics theory," *Journal of Applied Physics*, vol. 121, no. 12, p. 124902, 2017.
[11] A. Oliner and A. Hessel, "Guided waves on sinusoidally-modulated reactance surfaces," *IRE Transactions on Antennas and Propagation*, vol. 7, no. 5, pp. 201–208, 1959.
[12] S. Elnaggar and G. Milford, "Three wave mixing as the limit of nonlinear dynamics theory for nonlinear transmission line type metamaterials," *IEEE Transactions on Antennas and Propagation*, vol. 66, no. 1, 2018.
[13] Z. Yu and S. Fan, "Complete optical isolation created by indirect interband photonic transitions," *Nat Photon*, vol. 3, no. 2, pp. 91–94, 2009.
[14] H. Lira, Z. Yu, S. Fan, and M. Lipson, "Electrically driven nonreciprocity induced by interband photonic transition on a silicon chip," *Phys. Rev. Lett.*, vol. 109, p. 033901, Jul 2012.
[15] D. L. Sounas, C. Caloz, and A. Alù, "Giant non-reciprocity at the subwavelength scale using angular momentum-biased metamaterials," *Nature Communications*, vol. 4, p. 2407, 2013.

[16] J. N. Winn, S. Fan, J. D. Joannopoulos, and E. P. Ippen, "Interband transitions in photonic crystals," *Phys. Rev. B*, vol. 59, pp. 1551–1554, Jan 1999.
[17] Y. Hadad, J. C. Soric, and A. Alu, "Breaking temporal symmetries for emission and absorption," *Proceedings of the National Academy of Sciences*, vol. 113, no. 13, pp. 3471–3475, 2016.
[18] S. Taravati and C. Caloz, "Mixer-duplexer-antenna leaky-wave system based on periodic space-time modulation," *IEEE Transactions on Antennas and Propagation*, vol. 65, no. 2, pp. 442–452, 2017.
[19] S. Qin, Q. Xu, and Y. E. Wang, "Nonreciprocal components with distributedly modulated capacitors," *IEEE Transactions on Microwave Theory and Techniques*, vol. 62, no. 10, pp. 2260–2272, 2014.
[20] N. A. Estep, D. L. Sounas, and A. Alù, "Magnetless microwave circulators based on spatiotemporally modulated rings of coupled resonators," *IEEE Transactions on Microwave Theory and Techniques*, vol. 64, no. 2, pp. 502–518, 2016.
[21] C. N. Taravati, Sajjad and C. Caloz, "Nonreciprocal electromagnetic scattering from a periodically space-time modulated slab and application to a quasi-sonic isolator," *arXiv:1705.06311*, 2017.
[22] C. Caloz, K. Achouri, Y. Vahabzadeh, and N. Chamanara, "Spacetime metasurfaces," in *2016 Photonics North (PN)*, May 2016, pp. 1–2.
[23] G. Trainiti and M. Ruzzene, "Non-reciprocal elastic wave propagation in spatiotemporal periodic structures," *New Journal of Physics*, vol. 18, no. 8, p. 083047, 2016.
[24] Y. Hadad, D. L. Sounas, and A. Alú, "Space-time gradient metasurfaces," *Phys. Rev. B*, vol. 92, p. 100304, Sep 2015.
[25] E. S. Cassedy, "Temporal instabilities in traveling-wave parametric amplifiers (correspondence)," *IRE Transactions on Microwave Theory and Techniques*, vol. 10, no. 1, pp. 86–87, January 1962.
[26] C. Croënne, J. Vasseur, O. Bou Matar, M.-F. Ponge, P. Deymier, A.-C. Hladky-Hennion, and B. Dubus, "Brillouin scattering-like effect and non-reciprocal propagation of elastic waves due to spatio-temporal modulation of electrical boundary conditions in piezoelectric media," *Applied Physics Letters*, vol. 110, no. 6, p. 061901, 2017.
[27] W. H. Louisell. New York, Wiley, 1960, (William Henry).
[28] J. R. Pierce, "Coupling of modes of propagation," *Journal of Applied Physics*, vol. 25, no. 2, 1954.
[29] A. Taflove and S. C. Hagness, *Computational electrodynamics: the finite-difference time-domain method*. Artech house, 2005.
[30] J. B. Schneider, "Understanding the finite-difference time-domain method," *School of electrical engineering and computer science Washington State University.–URL: www.eecs.wsu.edu/ schneidj/ufdtd/ufdtd.pdf*", 2010.
[31] A. Taflove and S. C. Hagness, *Computational electrodynamics*. Artech house publishers, 2000.

Sameh Elnaggar Sameh received his B.Sc (Electrical Engineering) and M.Sc (Electrical Engineering) from Alexandria University, Egypt, and a PhD (Electrical and Computer Engineering) from the University of New Brunswick (UNB), Canada. He worked as a postdoctoral fellow at UNB, ACERT, Cornell University in conjunction with UNB and at the School of Engineering & Information Technology, University of New South Wales. Currently he is a Visiting Researcher at Royal Military College of Canada and works as an Electrical Engineer at Semtech Inc., Ottawa, where he is modelling and characterizing high speed circuits, interconnects and packages. He has industrial experience in automatic control, interferometry, EM modelling, high speed circuits and systems modelling. Sameh's research interests are in Nonlinear Metamaterials, Space-time structures, Wireless Power Transfer and Modelling of High Speed circuits.

Gregory Milford Greg Milford received the BE degree in Electrical Engineering from the University of Queensland (1979) and MEngSc (1992) and PhD degrees from the University of New South Wales (2002). Since January 2000 he has been a member of academic staff in the School of Engineering & Information Technology, UNSW, at the Australian Defence Force Academy in Canberra. His research interests focus on analysis and design of metamaterial structures for circuit and antenna applications, techniques for modeling devices and planar structures, and analysis and design of antennas in conducting media. He teaches classes on circuit theory, electronics and engineering electromagnetics. He also has extensive experience working in industry on the design, development, maintenance and implementation of a range of RF circuits and systems.